



# Coil Ambient Temperature and Its Influence on the Formation of Blocking Layer in the Electromagnetic Induction-Controlled Automated Steel-Teeming System

Ming He<sup>1,2</sup> · Xian-Liang Li<sup>1,3</sup> · Xing-An Liu<sup>1</sup> · Xiao-Wei Zhu<sup>1,2</sup> · Tie Liu<sup>1</sup> · Qiang Wang<sup>1</sup>

Received: 10 September 2018 / Revised: 21 September 2018 / Published online: 12 October 2018  
© The Chinese Society for Metals and Springer-Verlag GmbH Germany, part of Springer Nature 2018

## Abstract

Ambient temperature of induction coil is an important factor to influence the implementation of the electromagnetic induction-controlled automated steel-teeming (EICAST) technology. Meanwhile, it also affects the formation of Fe–C alloy blocking layer, which determines the length and installation position of induction coil. An experimental platform was designed to imitate actual working conditions in a ladle with the EICAST system. Ambient temperature of induction coil under high-temperature condition was measured to verify the accuracy of numerical result. After containing molten steel for 120 min and steel teeming for 40 min, the ambient temperature on the upper side of induction coil is 791 °C. In addition, the position of blocking layer in a 110 t ladle was measured by sand-collection and steel-pour methods, and the criterion temperatures of blocking layer in numerical simulation process were corrected. When the refining temperature is 1600 °C and the containing time of molten steel is 120 min, the thickness of blocking layer is 130 mm, and the distance between the upper surface of blocking layer and the upper surface of nozzle brick is 154 mm. When the criterion temperatures are 919 °C and 428 °C, the numerical results can be used to confirm the position of blocking layer and the installation position of induction coil.

**Keywords** Clean steel · EICAST technology · Heat transfer · Blocking layer · Coil ambient temperature

## 1 Introduction

Steel with excellent work performance is the ultimate goal for many metallurgical scholars and steel enterprises [1]. Steel cleanliness has a significant effect on the steel microstructure, which further affects the ultimate performance of steel [2, 3]. After proposing the concept of clean steel, many clean steel production technologies are put forward and industrialized to reduce inclusion content and

size in steel, such as the hot metal desulphurization, the top and bottom combined converter blowing, the slag detection, and the argon stirring [4–7]. During the steel-teeming process, the removal or optimization of nozzle sand is a hot research topic of clean steel production. In a sliding gate system, the nozzle sand, a foreign inclusion, will drop into a tundish within molten steel. Studies have shown that the number of large-size Al<sub>2</sub>O<sub>3</sub> inclusions in molten steel will decrease after pouring into the tundish from the ladle [8]. The number of small-size Al<sub>2</sub>O<sub>3</sub> inclusions will increase obviously at that process, and the mixture of nozzle sand and other refractory materials is an important reason. To reduce the nozzle sand dropped into the tundish, many metallurgical workers have carried out lots of research works [9, 10]. Typically, Yang [9] puts forward a new method of setting a recovery device of nozzle sand near the lower nozzle. After opening the lower slide gate, the recovery device is moved to the position, where the nozzle sand falls. Liu [10] proposed a new method of using high-pressure gas under the lower nozzle to blow the nozzle sand away from long nozzle or tundish. Although the two

Available online at <http://link.springer.com/journal/40195>

✉ Qiang Wang  
wangq@mail.neu.edu.cn

<sup>1</sup> Key Laboratory of Electromagnetic Processing of Materials (Ministry of Education), Northeastern University, Shenyang 110819, China

<sup>2</sup> School of Metallurgy, Northeastern University, Shenyang 110819, China

<sup>3</sup> School of Materials Science and Engineering, Northeastern University, Shenyang 110819, China

methods mentioned above can reduce the nozzle sand dropped into the tundish, their operation is inconvenient to control, and they will affect the pace of automatic production seriously. More serious problem is that they will increase the possibility of production accidents.

The automatic free-opening rate is also another important factor affecting the automated production in steel enterprises [11–13]. For crude steel in continuous casting production, the automatic free-opening rate can reach about 98%. However, the automatic free-opening rate of special steel is only about 80%. When the ladle is not opened automatically, an oxygen burning method will be applied to assist the opening. This will not only disturb the production rhythm, but also cause the secondary oxidation of molten steel. The reasons for the failure of automatic free opening include the filling state, the composition and particle shape of nozzle sand [14, 15]. It is found that the automatic free-opening rate of ladle can be increased by improving the filling state of nozzle sand in the nozzle, optimizing the composition of nozzle sand, or improving the masonry structure at the bottom of ladle, but it is difficult to increase the automatic free-opening rate greatly or even to 100% [16–18].

An electromagnetic induction-controlled automated steel-teeming (EICAST) technology has attracted much attention, because it can solve the problems mentioned above in the sliding gate system [19–21]. In the EICAST system, Fe–C alloy particle is used as a new filling material to replace nozzle sand. The composition of Fe–C alloy is similar to that of liquid steel. After pouring high-temperature molten steel into ladle, Fe–C alloy particles in the upper nozzle will be divided into four layers from top to bottom because of heat transfer from molten steel. They are the melted layer, liquid-sintered layer, solid-sintered layer, and original layer, respectively. Liquid-sintered layer and solid-sintered layer have contribution to block liquid steel, known as the blocking layer [22]. When the ladle is placed at the pouring position, the process is to melt whole or part Fe–C blocking layer by Joule heat generated by induction coil. Electromagnetic induction heating is applied in the steel-teeming process by the EICAST technology successfully. This method can avoid using nozzle sand. And the automatic free-opening rate can also reach 100% by this new technology.

The feasibility of the EICAST technology was verified by laboratory experiments [23]. To apply this new technology in the industrial production, a large number of numerical simulations had been carried out [24]. Design and operating parameters of the EICAST system aimed at a large ladle were determined and calculated. Safety and reliability of the new ladle with the EICAST system were also investigated. However, during the industrial tests, whether the coil material is pure copper or Cu–0.6Cr–0.2Zr

alloy [25], ambient temperature affects the working performance of induction coil seriously, and it also affects coil structure design and insulation method. Induction coil cannot be cooled by water because it is located at the bottom of ladle. In addition, the coil ambient temperature also affects the formation of Fe–C alloy blocking layer, which is directly related to the length and installation position of induction coil. Therefore, it is necessary to measure the coil ambient temperature, and the position and thickness of Fe–C alloy blocking layer by experiments.

In this work, a large experimental platform was designed to imitate the actual working conditions of the EICAST system, and the coil ambient temperatures were measured. Moreover, the position of Fe–C alloy blocking layer in a 110 t ladle were measured by sand-collection method and steel-pour method. Finally, the experimental results were compared with simulation results. These studies are helpful to analyze the length and installation position of induction coil and to promote the industrial application of the EICAST system.

## 2 Experimental

### 2.1 Design of Experimental Platform

In the EICAST system, induction coil is directly embedded in nozzle brick at the bottom of the ladle. As a new filling material, the Fe–C alloy particles are placed into the upper nozzle before containing molten steel. Because of heat transfer from molten steel, Fe–C alloy particles will form a blocking layer. At the same time, the ambient temperature of the induction coil will increase gradually, which affects the service life of the induction coil. To imitate the actual

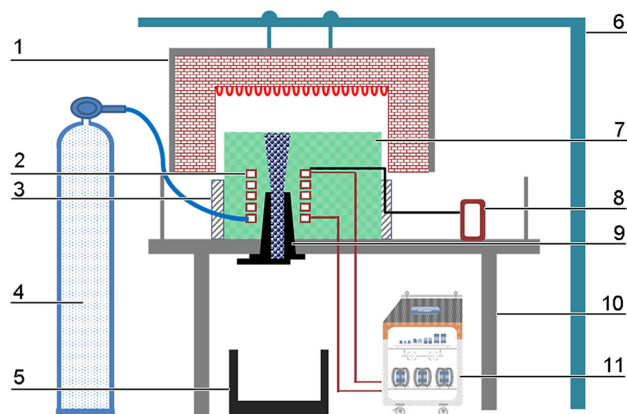


**Fig. 1** Schematic illustration of electromagnetic steel-teeming experimental devices. 1—resistance furnace; 2—induction coil; 3—thermal insulation material; 4—compressed air; 5—collecting device; 6—support structure; 7—nozzle brick; 8—K thermocouple; 9—upper nozzle; 10—experimental platform; 11—induction power supply

working conditions in the ladle, a large experimental platform is designed, as shown in Fig. 1. The nozzle brick with an induction coil used in this device has the same size and material with the nozzle brick used in the ladle of a steel plant. By resistance heating, the upper surface temperature of nozzle brick can reach 1600 °C, which is used to simulate the high temperature from liquid steel. Heating curve is designed according to the operation process of the ladle in the steel plant. According to the heating curve, the upper surface of nozzle brick is heated and maintained high temperature for a period of time. At that time, the coil ambient temperatures can be measured.

During the experimental process, the Fe–C alloy particles were filled in the upper nozzle firstly, and the composition of Fe–C alloy particles is shown in Table 1. Then, the resistance furnace was fallen to a fixed position. At that time, the distance between the upper surface of nozzle brick and heating elements in resistance furnace was 15 mm. Four sides of nozzle brick were wrapped by heat preservation material of thickness 80 mm. Finally, the resistance furnace was turned on. After that, the upper surface temperature of nozzle brick reached 1600 °C and maintained 120 min, and the temperature on the upper side of induction coil was measured by a K thermocouple.

## 2.2 Sand-Collection Method and Steel-Pour Method

In order to measure the position and thickness of Fe–C alloy blocking layer in the 110 t ladle used in the steel plant, as shown in Figs. 2 and 3, sand-collection method and steel-pour method were proposed. Different steel grades need different refining temperatures. Therefore, the selected refining temperatures were 1500 °C and 1600 °C in experiments, respectively. The composition of Fe–C alloy particles is also shown in Table 1.

By using sand-collection method, the lower surface position of Fe–C alloy blocking layer can be calculated by original Fe–C alloy particles collected after opening the sliding gate. As shown in Fig. 2b, the original Fe–C alloy particles were collected and placed in a measuring device, and then, the values of  $d_1$  and  $d_2$  were measured. The length of the measuring ruler and total height of Fe–C alloy are  $d_1$ , and its value is 515 mm. The height of Fe–C alloy original layer is  $d_2$ , so the lower surface position of Fe–C alloy blocking layer can be determined by  $d_2$ .

In the steel-pour method, the molten steel in ladle after normal operation is poured into another empty ladle, the

melting layer of Fe–C blocking layer will flow out with the molten steel, and then the upper surface position of Fe–C alloy blocking layer can be measured directly, as shown in Fig. 3. In measuring stage, two pipes of length of 10 m through a fixed support were put into the upper nozzle and the nozzle brick, respectively. Length difference  $D_1$  is the distance between the upper surface of nozzle brick and the upper surface of Fe–C alloy blocking layer, which can characterize the thickness of Fe–C alloy melted layer. At the same time, another two pipes of length of 1 m through a fixed support were put into the upper nozzle and the bottom shell of ladle, respectively. Length difference  $D_2$  is the distance between the lower surface of Fe–C alloy blocking layer and the bottom shell of ladle, which can characterize the thickness of Fe–C alloy original layer. The distance between the upper surface of nozzle brick and the bottom shell of ladle is  $D_0$ . Thus, the thickness of Fe–C alloy blocking layer can be calculated by  $D_0 - D_1 - D_2$ .

## 3 Numerical Simulation

Finite element analysis model in numerical simulation was built according to the actual nozzle brick and induction coil, as shown in Fig. 4a. Relevant dimensions are shown in Fig. 4b. After the ladle with the EICAST system runs several cycles, the temperature distribution inside nozzle brick reaches thermal saturation and the coil ambient temperature reaches maximum value.

Because of the complexity of the EICAST system, some necessary assumptions are as follows:

1. The material of the upper nozzle is the same as that of nozzle brick, and the gap between the upper nozzle and nozzle brick is neglected.
2. The composition of Fe–C alloy particles is the same as that of molten steel. The Fe–C alloy particles are well packed in the upper nozzle, and the gaps between Fe–C alloy particles are neglected.
3. When calculating the ambient temperature of induction coil and the position of Fe–C alloy blocking layer, the upper surface temperature of nozzle brick is 1600 °C; during the steel-teeming period, the upper surface temperature of nozzle brick and the inner surface of the upper nozzle are 1600 °C.
4. Because the induction coil moves along with the ladle before steel teeming, the coil is not cooled by forced air cooling, so induction coil is filled with still air, and the convective coefficient of still air is  $5 \text{ W}/(\text{m}^2 \text{ } ^\circ\text{C})$ .

**Table 1** Composition of Fe–C alloy particles

Fe–C alloy	C	Si	Mn	P	S	Cu	Ni
Components	0.07–0.13	0.17–0.37	0.35–0.65	≤ 0.035	≤ 0.035	≤ 0.25	≤ 0.25

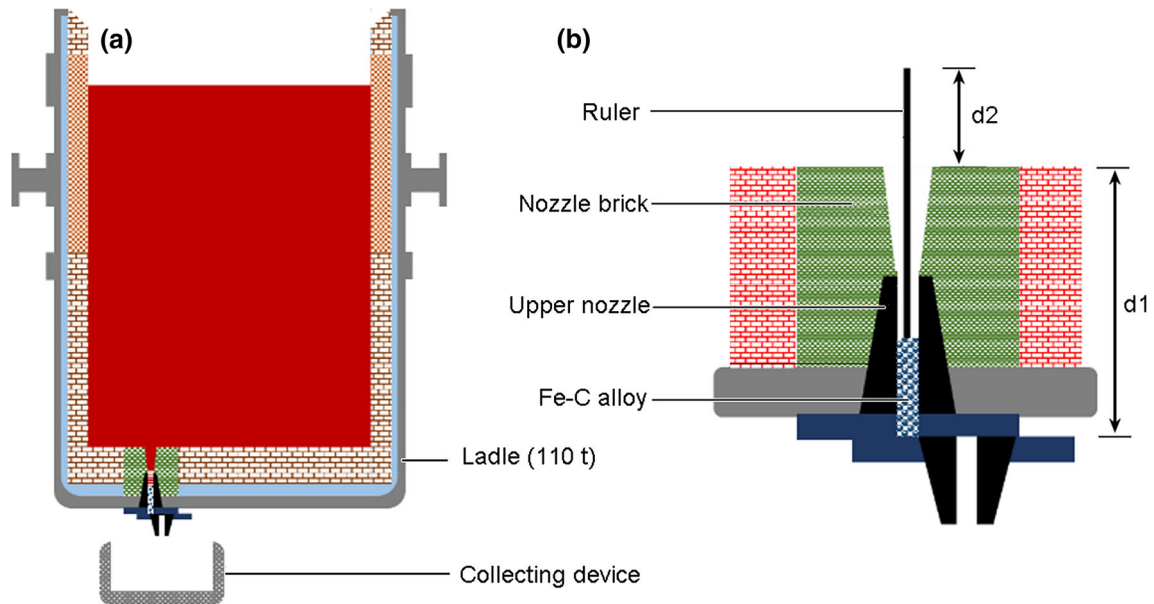


Fig. 2 Schematic illustration of sand-collection method: **a** collecting device, **b** measuring device

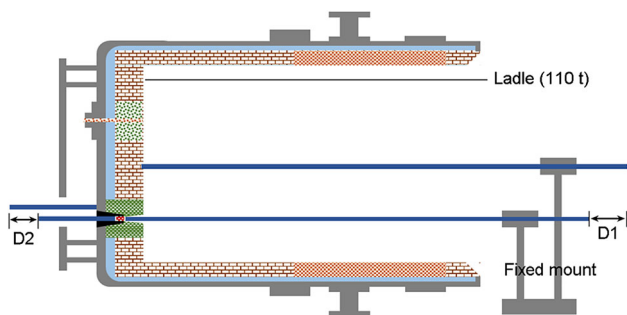


Fig. 3 Schematic illustration of steel-pour method

Four sides of nozzle brick are adiabatic; there is thermal convection between the lower surface of nozzle brick and air, and the convective coefficient is  $15 \text{ W}/(\text{m}^2 \text{ }^\circ\text{C})$ .

Physical parameters of all materials are shown in Table 2. As seen in Ref. [26], the specific heat capacity of

high alumina refractories is very little affected by temperature, so the specific heat capacity of nozzle brick is  $1.13 \text{ kJ kg}^{-1} \text{ }^\circ\text{C}^{-1}$ . The relationship between the thermal conductivity and temperature of nozzle brick is  $\lambda = 2.9 + 0.00019T$ , and the influence of temperature on the thermal conductivity is very small. Therefore, the selected thermal conductivity of nozzle brick is  $2.9 \text{ W m}^{-1} \text{ }^\circ\text{C}^{-1}$ . The specific heat capacity and thermal conductivity of Fe-C alloy at different temperatures are shown in Fig. 5. Similarly, the specific heat capacity and thermal conductivity of copper coil at different temperatures are shown in Fig. 6 [27].

For the three-dimensional heat conduction problem, the temperature distribution in the nozzle brick can be calculated by the following equation:

$$\rho c \frac{\partial T}{\partial \tau} = \frac{\partial}{\partial x} \left( \lambda \frac{\partial T}{\partial x} \right) + \frac{\partial}{\partial y} \left( \lambda \frac{\partial T}{\partial y} \right) + \frac{\partial}{\partial z} \left( \lambda \frac{\partial T}{\partial z} \right) + q_v$$

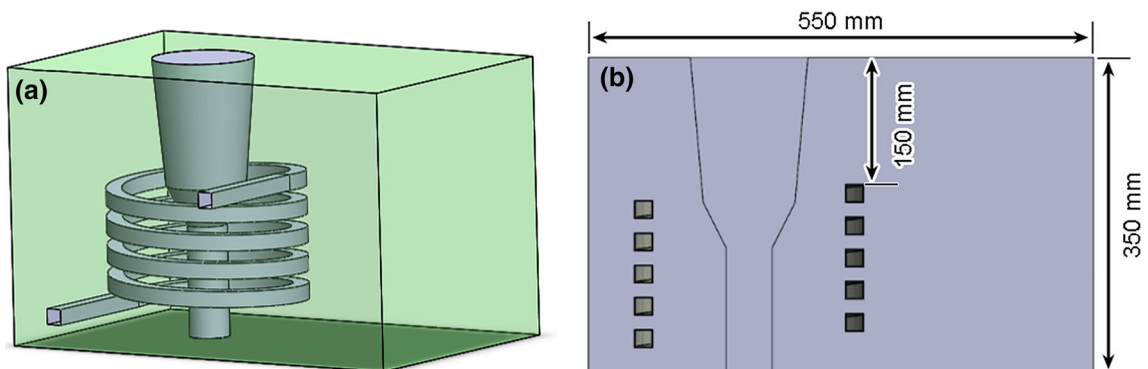
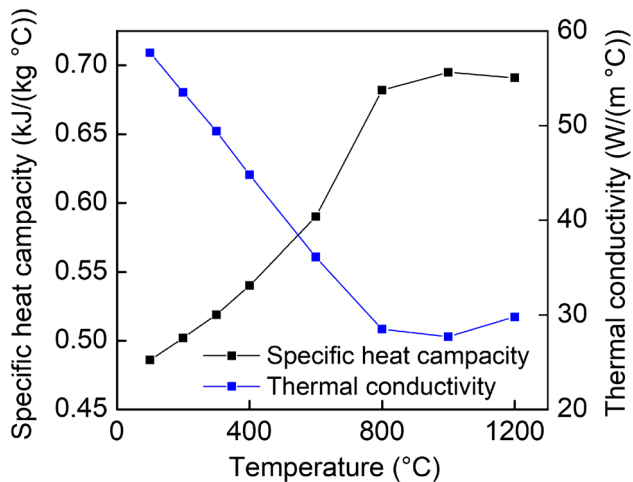
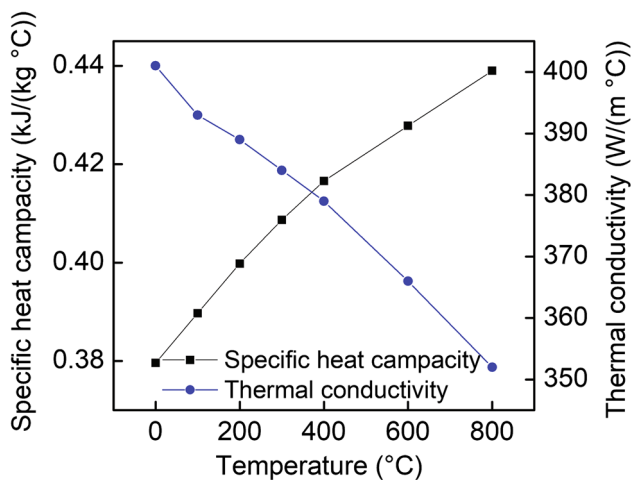


Fig. 4 Simulation model: **a** three-dimensional model, **b** relevant dimensions

**Table 2** Physical parameters of several materials

Materials	Density ( $\text{kg m}^{-3}$ )	Specific heat capacity ( $\text{kJ kg}^{-1} \text{ }^\circ\text{C}^{-1}$ )	Thermal conductivity ( $\text{W m}^{-1} \text{ }^\circ\text{C}^{-1}$ )
Nozzle brick	3040	1.13	2.9
Fe–C alloy	7830	Fig. 5	Fig. 5
Coil (copper)	8930	Fig. 6	Fig. 6

**Fig. 5** Specific heat capacity and thermal conductivity of Fe–C alloy**Fig. 6** Specific heat capacity and thermal conductivity of copper coil

where  $T$  is the temperature,  $^\circ\text{C}$ ;  $\lambda$  is the thermal conductivity,  $\text{W}/(\text{m } ^\circ\text{C})$ ;  $\rho$  is the material density,  $\text{kg}/\text{m}^3$ ;  $c$  is the specific heat capacity,  $\text{kJ}/(\text{kg } ^\circ\text{C})$ ;  $q_v$  is the internal heat source intensity,  $\text{W}/\text{m}^3$ ;  $\tau$  is the time, s. In this paper, only the positions and thickness of Fe–C alloy blocking layer are calculated by numerical simulation and the induction heating is not involved, so the internal heat source  $q_v = 0$ .

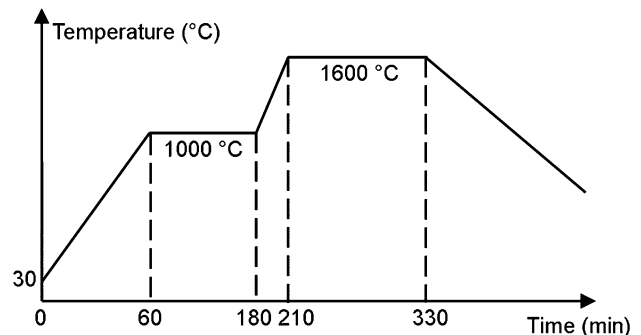
## 4 Results and Discussion

### 4.1 Measurement and Numerical Analysis of Coil Ambient Temperature

#### 4.1.1 Heating Curve Design and Model Validation

A ladle has to go through several stages during the actual production process in the steel plant: They are the ladle preheating stage, the containing molten steel stage, the refining stage, the standing and steel-teeming stage. In the preheating stage, the upper surface temperature of nozzle brick is  $1000\text{ }^\circ\text{C}$  approximately, and this stage lasts 120 min. After containing molten steel, the upper surface temperature of nozzle brick will reach  $1600\text{ }^\circ\text{C}$ , and this temperature will last 120 min until the steel-teeming stage starts. The steel-teeming time is 40 min. Therefore, to simulate the working condition, it is necessary to design an experimental heating curve for resistance furnace, as shown in Fig. 7. Firstly, the upper surface of nozzle brick is heated, the upper surface temperature of nozzle brick reaches  $1000\text{ }^\circ\text{C}$  after 60 min, and the heat preservation time is 120 min. After that, the upper surface of nozzle brick is heated to  $1600\text{ }^\circ\text{C}$  after 30 min. After keeping this temperature for 120 min, the maximal coil ambient temperature before the steel-teeming stage can be measured. After the measurement, the nozzle brick is cooled to room temperature naturally.

To verify the correctness of the numerical analysis model, this model was used to calculate the coil ambient temperature before steel-teeming stage. At the same time,

**Fig. 7** Temperature curve of the upper surface of nozzle brick



the coil ambient temperatures were measured by a  $K$  thermocouple in the experiment. Experimental results are compared with numerical simulation results, as shown in Fig. 8. We can find that the change trend of numerical simulation results is consistent with that of experimental results, so the simulation model can be used to predict other process parameters.

In addition, from Fig. 8, the temperature growth rate on the upper side of induction coil increases gradually in the heating stage (Fig. 8a, c), and the main reason of this phenomenon is the large temperature difference caused by a rapid growth of the upper surface temperature of nozzle brick. In heat preservation stages (Fig. 8b, d), the temperature growth rate on the upper side of induction coil decreases gradually. The reason is that temperature distribution of the nozzle brick tends to thermal saturation because the upper surface temperature of nozzle brick is an invariant constant.

#### 4.1.2 Coil Ambient Temperatures Before Steel Teeming and After Steel Teeming

After containing molten steel in the ladle, the coil ambient temperature increases continuously because of heat transfer from the high-temperature molten steel. When the containing time of molten steel is 120 min ( $t = 330$  min), the temperature distribution of nozzle brick is shown in Fig. 9. It can be concluded that the temperature distribution from top to bottom in nozzle brick is gradient according to the calculation results. The heat conduction in Fe–C alloy particles is faster than that of nozzle brick, because the thermal conductivity of Fe–C alloy is larger than that of nozzle brick. At this time, the upper surface temperatures of induction coil obtained by numerical calculation and experimental measurement are 626 and 667 °C, respectively. The numerical result is less than the experimental one slightly. The main reason is that there is a gap between

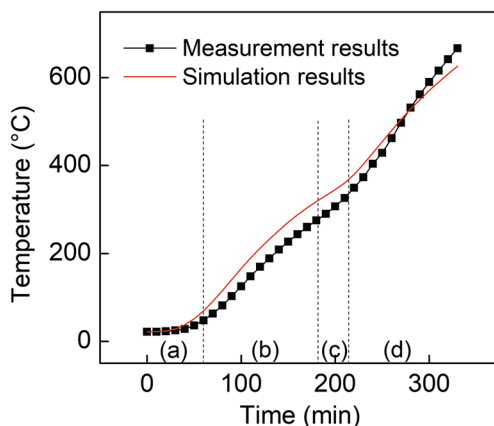


Fig. 8 Temperature variation curve of coil ambient temperature

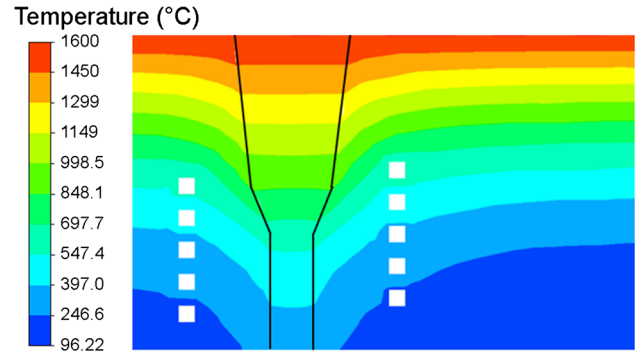


Fig. 9 Temperature distribution inside nozzle brick before steel teeming ( $t = 330$  min)

four sides of nozzle brick and resistance furnace in the experiments, so four sides of nozzle brick will be heated at the same time when the upper surface of nozzle brick is heated. However, the four sides of nozzle brick are adiabatic during the simulation process. In the industrial test process, the errors caused by the above factors can be neglected. And as shown in Fig. 8, the errors between numerical results and experimental results are very small. Therefore, the numerical simulation method can predict the upper side temperature of induction coil in the nozzle brick.

After automatic steel teeming, high-temperature molten steel flows through nozzle brick and upper nozzle into the tundish. The working condition of induction coil will become worse, and the coil ambient temperature increases furtherly. As mentioned earlier, numerical simulation method can also calculate the coil ambient temperature approximately. Therefore, the temperature distribution of nozzle brick after molten steel containing time for 120 min and steel-teeming time for 40 min ( $t = 370$  min) is shown in Fig. 10. At this time, the upper side temperature of induction coil is 791 °C, which is very important to guide heat insulation and cooling of induction coil.

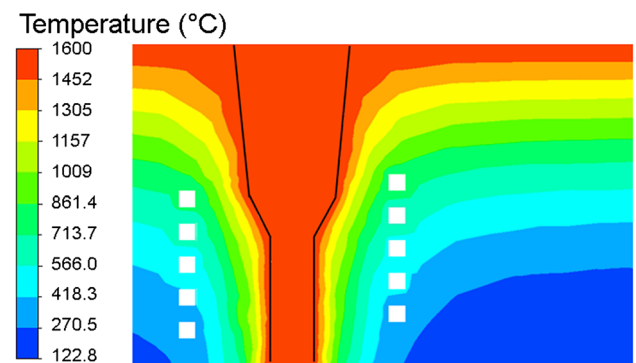


Fig. 10 Temperature distribution inside nozzle brick after steel teeming

## 4.2 Analysis of Position and Thickness of Fe–C Alloy Blocking Layer

Refining temperature of different steel grades is different. And the containing time of molten steel in ladle also affects the temperature distribution of nozzle brick. These will affect the coil ambient temperature seriously and also affect the position and thickness of the Fe–C alloy blocking layer. When the refining temperature of liquid steel was 1600 °C, and the containing time of molten steel in ladle was 120 min, the position and thickness of the Fe–C alloy blocking layer were measured by sand-collection method and steel-pour method in industrial experiments. They were also calculated by numerical simulation. The experimental results are compared and analyzed with numerical results. After that, the criterion temperatures of the Fe–C alloy blocking layer are corrected in numerical calculation.

### 4.2.1 Experimental Results of Position and Thickness of Fe–C Alloy Blocking Layer

The cost of sand-collection method is low, and this method has no influence on the normal steel production process. Therefore, this method is used to measure the height of the Fe–C alloy original layer during the experimental process. When refining temperatures are 1500 and 1600 °C, the results are shown in Fig. 11. The shape of the Fe–C alloy particles is cylindrical, and their sizes are 2.0 mm:2.0 mm (bottom diameter to height). The average height of the Fe–C alloy original layer is 243 mm when refining temperature of molten steel is 1500 °C. That means that the distance between the lower surface of the blocking layer and the bottom of the upper slide plate is 243 mm. Similarly, when refining temperature of molten steel is 1600 °C, the average height of the Fe–C alloy original layer is 231 mm.

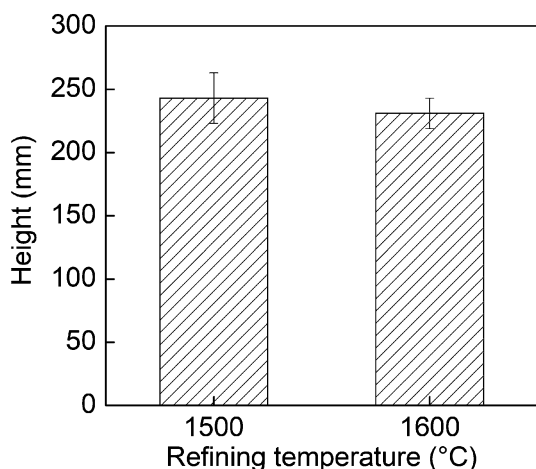


Fig. 11 Height of the Fe–C alloy original layer at different refining temperatures

Obviously, the position of the Fe–C alloy blocking layer moves downward with the increase of refining temperature of liquid steel.

The lower surface position of the Fe–C alloy blocking layer can be measured by the sand-collection experiments, but the top surface position and thickness of the Fe–C alloy blocking layer cannot be obtained by this method. In the sand-collection experiments, the lower surface position of the Fe–C alloy blocking layer is lower relatively when refining temperature of molten steel is 1600 °C. Therefore, the position of induction coil in the EICAST system needs to be designed according to a lower surface position of the blocking layer. After that, the EICAST system can be applied in all steel grades during the steel production process. Because of its high cost, the steel-pour method was only used to investigate the position and thickness of the Fe–C alloy blocking layer when the refining temperature of molten steel is 1600 °C. The experimental results show that the height  $D_1$  of the Fe–C alloy melting layer is 154 mm, which means that the 154-mm Fe–C alloy particles at the top of the upper nozzle are melted completely. The height  $D_2$  of the Fe–C alloy original layer is 231 mm, which means that the 231-mm Fe–C alloy particles at the bottom of the upper nozzle are not sintered, and they can fall freely after the sliding gate is opened. Therefore, the thickness of the Fe–C alloy blocking layer can be calculated, and it is 130 mm. The results are consistent with those obtained by sand-collection method. Based on the above results, the position and thickness of the Fe–C alloy blocking layer can be obtained, as shown in Fig. 12.

### 4.2.2 Numerical Analysis of Fe–C Alloy Blocking Layer

Temperature distribution of Fe–C alloy is gradient because of heat transfer from high-temperature molten steel in ladle. The temperature of Fe–C alloy increases with the increase of containing time of molten steel. Therefore, the temperature distributions at the centerline of Fe–C alloy after different containing time of molten steel were

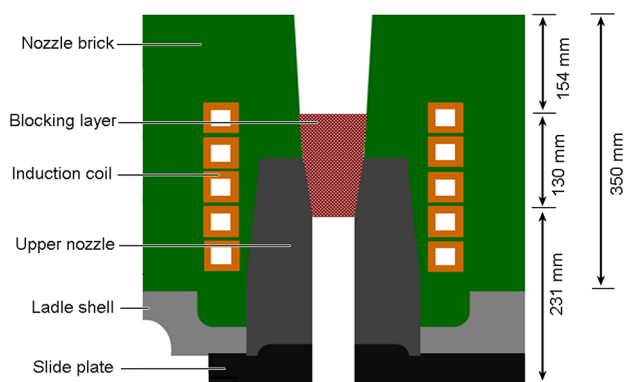


Fig. 12 Position and thickness of the Fe–C alloy blocking layer

calculated by numerical simulation, as shown in Fig. 13. With the increase of containing time of molten steel, the temperature of Fe–C alloy increases gradually, but the growth rate of temperature decreases gradually. Compared with the temperature of Fe–C alloy when the containing time of molten steel is 120 min ( $t = 330$  min), the temperature rise of Fe–C alloy is not obvious when the containing time of molten steel is 180 min ( $t = 390$  min).

In addition, it can be found from Fig. 13, when the containing time of molten steel is 120 min ( $t = 330$  min), the temperature distribution from top to bottom of Fe–C alloy is gradient because of heat conduction from high-temperature molten steel. Melting point of Fe–C alloy in Table 1 is 1505 °C, and sintering temperature of Fe–C alloy is 900 °C [28]. If the melting point and sintering temperature of Fe–C alloy are used as criterion standard to confirm the position and thickness of Fe–C alloy blocking layer, the thickness of blocking layer is 127 mm, the distance between the top surface of blocking layer and the top surface of nozzle brick is 31 mm, and the distance between bottom surface of blocking layer and bottom surface of nozzle brick is 192 mm. Compared with the results obtained by sand-collection method and steel-pour method, these results about Fe–C alloy blocking layer have a big difference. Therefore, according to the experimental results, it is necessary to correct the criterion temperatures of Fe–C alloy blocking layer after numerical calculation.

The reasons for the difference between the experimental results and simulation results are shown in Fig. 14. After the heat transfer from liquid steel, there is an Fe–C alloy transition layer between melted layer and sintered layer. And the temperature of the transition layer is lower than the melting point of Fe–C alloy particles in numerical simulation. However, the transition layer is mainly composed of

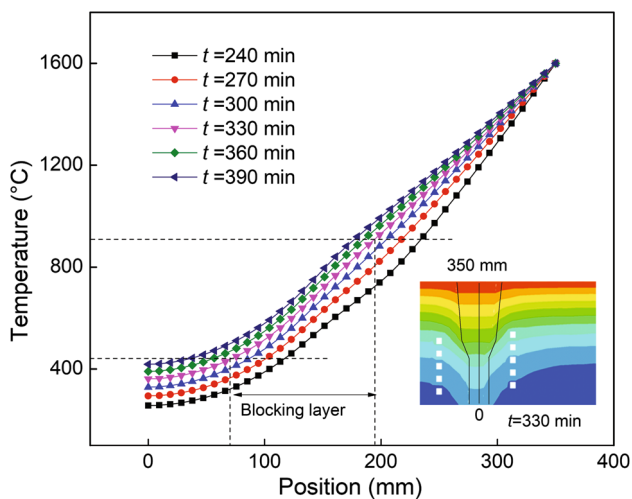


Fig. 13 Temperature variation of Fe–C alloy at different time

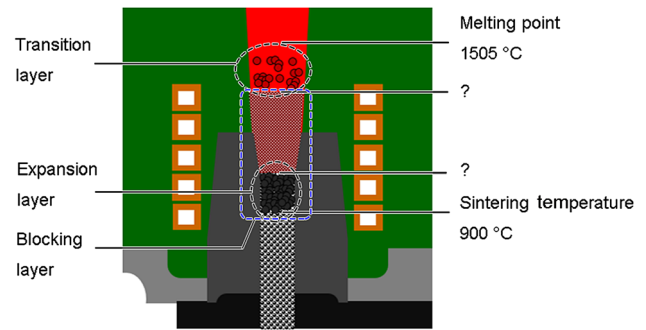


Fig. 14 Mechanism analysis of thickness and position difference of blocking layer

Fe–C alloy particles, interstitial molten steel, and Fe–C alloy sintered clusters, which cannot block the molten steel. In the steel-pour experiments, the Fe–C alloy transition layer will flow out with liquid steel. Therefore, it is wrong to determine the upper surface position of the blocking layer by the melting point of Fe–C alloy. However, because of the limited experimental conditions, the Fe–C alloy transition layer cannot be measured. For the lower surface of the blocking layer, when the ambient temperature exceeds a certain value, the Fe–C alloy particles will expand and the friction between them will increase, which lead to a result that the expanded Fe–C alloy particles cannot fall down automatically. After opening the sliding gate, under the sintering layer, there are some expanded Fe–C alloy particles, which cannot drop automatically, and they are also a part of blocking layer. There is an Fe–C alloy expansion layer between sintered layer and original layer. Therefore, the lower surface position of the Fe–C alloy blocking layer cannot be determined by the Fe–C alloy sintering temperature. Compared with the experimental results, after numerical calculation, the criterion temperatures of Fe–C alloy blocking layer are 919 °C (the upper surface temperature of blocking layer) and 428 °C (the lower surface temperature of blocking layer), as shown in Fig. 15. By these criterion temperatures, the simulation results about position and thickness of the Fe–C alloy blocking layer are in agreement with the experimental results.

As mentioned earlier, the containing time of molten steel in ladle is an important factor affecting the position and thickness of the Fe–C alloy blocking layer. For different steel grades, the refining process and refining time are different, which leads to different containing time of molten steel. After different containing time of molten steel, the position and thickness of the Fe–C alloy blocking layer are shown in Fig. 16. It shows that with the increase of the containing time of molten steel, the position of the Fe–C alloy blocking layer moves downward gradually,



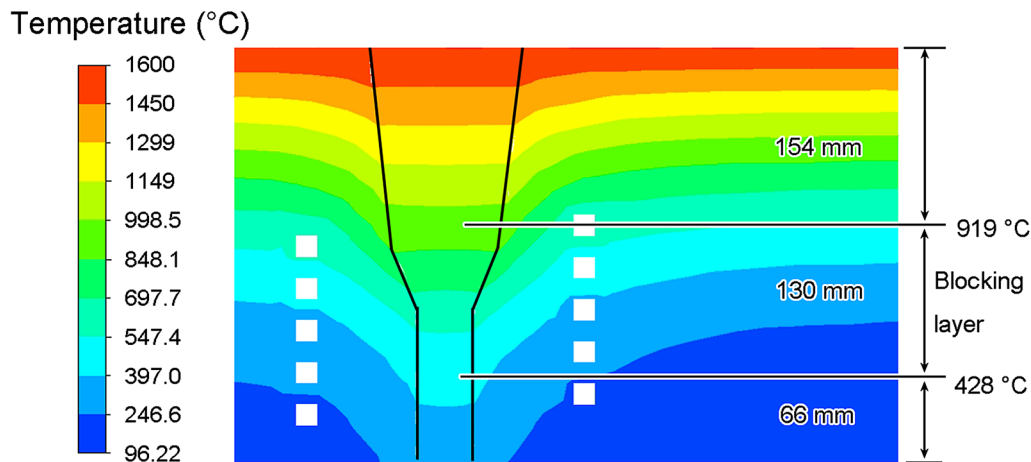


Fig. 15 Criterion temperatures of Fe–C alloy plugging layer

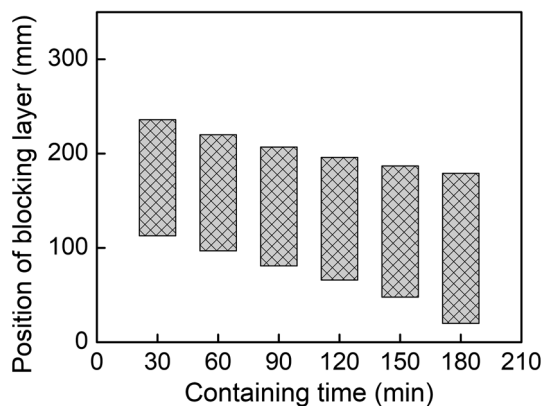


Fig. 16 Position of Fe–C alloy blocking layer after different containing time

which is beneficial to the installation of induction coil in nozzle brick. However, long containing time of molten steel will lead to an increase in the thickness of the blocking layer, which is detrimental to the installation of induction coil. Therefore, when the containing time of molten steel is too short or too long, the position and thickness of the Fe–C alloy blocking layer need to be adjusted by other ways. However, the C content in Fe–C alloy has a significant influence on the melting point of Fe–C alloy. With the increase of C content, the melting point of Fe–C alloy decreases obviously [29]. Therefore, when the containing time of molten steel is certain, the Fe–C alloy composition can be adjusted to ensure the position and thickness of the Fe–C alloy blocking layer within a suitable range, which can guide the installation of induction coil. These are important for the wide application of the EICAST technology.

## 5 Conclusions

By the experiments in the large experimental platform and in the steel plant, the coil ambient temperature and the position of Fe–C alloy blocking layer were measured. Numerical simulation results about those were also verified and corrected. Main conclusions are as follows:

1. Coil ambient temperature increases with the increase of containing time of molten steel in ladle. When the upper surface temperature of nozzle brick reaches 1600 °C and maintains 120 min, the upper surface temperature of induction coil will reach 626 °C.
2. After containing molten steel for 120 min and steel teeming for 40 min, the working environment of induction coil is the worst, and the coil ambient temperature will reach 791 °C, which provides a theoretical basis for the design of insulation and cooling.
3. By sand-collection method and steel-pour method, the position and thickness of Fe–C alloy blocking layer in a 110 t ladle were measured. The thickness of blocking layer is 130 mm, the distance between the upper surface of blocking layer and the upper surface of nozzle brick is 154 mm, and the distance between the lower surface of blocking layer and the lower surface of upper slide gate is 231 mm. Compared with the experimental results, the criterion temperatures of the Fe–C alloy blocking layer in numerical simulation are modified to 919 and 428 °C.
4. Containing time of molten steel can change the position and thickness of the blocking layer. The C content can be adjusted to change the melting point of the Fe–C alloy, and the position and thickness of the Fe–C alloy blocking layer can be adjusted by this way.

**Acknowledgements** This work was financially supported by the National Natural Science Foundation of China (Grant No. U1560207).

## References

- [1] Y. Hou, Z.Q. Zhang, W.D. Xuan, J. Wang, J.B. Yu, Z.M. Ren, *Acta Metall. Sin. (Engl. Lett.)* **31**, 681 (2018)
- [2] F.P. Tang, D.G. Li, X.W. Liao, X.F. Wang, X.F. Wan, J.X. Jia, J.G. Zhang, *J. Iron Steel Res. Int.* **18**, 9 (2011)
- [3] G.G. Cheng, M.L. Wang, X.E. Yang, Y.L. Li, Y.G. Wang, L.Y. Wang, P. Zhao, *Acta Metall. Sin. (Engl. Lett.)* **16**, 379 (2003)
- [4] H.J. Visser, R. Boom, *ISIJ Int.* **46**, 1771 (2006)
- [5] Z.Y. Lai, Z. Xie, L.C. Zhong, *ISIJ Int.* **48**, 793 (2008)
- [6] D.P. Tan, P.Y. Li, X.H. Pan, *J. Iron Steel Res. Int.* **16**, 1 (2009)
- [7] L. Cheng, W.G. Pang, K.Y. Peng, D.Z. Liu, W.Q. Shi, X.H. Peng, *China Metall.* **23**, 31 (2013)
- [8] L.F. Zhang, B.G. Thomas, X.H. Wang, K. Cai, in *85th Steel-making Conference Proceedings, ISS-AIME*, Warrendale, PA, vol. 431 (2002)
- [9] J. Yang, China Pat. CN104690241A (2015)
- [10] W.D. Liu, China Pat. CN102218527A (2011)
- [11] Y.L. Sun, Y.Z. Luo, X.C. Jia, *Cont. Cast.* **41**, 23 (2016)
- [12] Y.F. Huang, P.Y. Du, Y.S. Li, *Refract* **40**, 433 (2006)
- [13] F. Farshidfar, M.G. Kakroudi, *J. Iron. Steel Res. Int.* **19**, 11 (2012)
- [14] C. Zhang, Z. Li, L.Y. Zhu, Y.K. Xie, *Cont. Cast. (China)* **42**, 46 (2017)
- [15] J.H. He, W.D. Qiu, Y.H. Liang, J.H. Nie, Y.C. Yin, *Refract* **48**, 74 (2014)
- [16] J.H. Zhu, S.L. Chen, S.H. Zhou, H.P. Zhang, *Cont. Cast.* **4**, 43 (2005)
- [17] H.X. Zhu, C.J. Deng, C. Bai, W.G. Zhang, *Steelmaking* **24**, 49 (2008)
- [18] G.J. Wang, X.M. Li, Y.H. Pan, J. Hong, Z.B. Guo, M. Zhang, *Steelmaking* **23**, 24 (2007)
- [19] D.J. Li, Q. Wang, X.A. Liu, A. Gao, X.B. Wang, J. Dong, K. Marukawa, J.C. He, *J. Iron. Steel Res. Int.* **19**, 766 (2012)
- [20] Q. Wang, D.J. Li, X.A. Liu, X.B. Wang, J. Dong, J.C. He, *J. Iron. Steel Res. Int.* **22**, 30 (2015)
- [21] M. He, Q. Wang, X.A. Liu, C.Y. Shi, T. Liu, J.C. He, *High Temp. Mater. Proc.* **36**, 441 (2017)
- [22] Q. Wang, J.C. He, T. Liu, *New Technologies of Electromagnetic Metallurgy* (Science Press, Beijing, 2015), p. 90
- [23] A. Gao, Q. Wang, D.J. Li, B.G. Jin, K. Wang, J.C. He, *Acta Metall. Sin.* **46**, 634 (2010)
- [24] X.A. Liu, Q. Wang, D.J. Li, G.L. Li, D.Q. Geng, A. Gao, J.C. He, *ISIJ Int.* **54**, 482 (2014)
- [25] M. He, X.L. Li, Z.Q. Cao, S.L. Dong, T. Liu, Q. Wang, *Vacuum* **146**, 130 (2017)
- [26] W.H. Tong, F.M. Shen, H. Shibata, W.Z. Wang, Y.S. Yang, Y. Waseda, R. Takahashi, J.I. Yagi, *Acta Metall. Sin.* **38**, 983 (2002)
- [27] S.M. Yang, W.Q. Tao, *Heat Transfer* (Higher Education Press, Beijing, 2006), p. 555
- [28] A. Gao, D.J. Li, Q. Wang, K. Wang, B.G. Jin, K. Marukawa, J.C. He, *ISIJ Int.* **50**, 1770 (2010)
- [29] A. Gao, Q. Wang, D.J. Li, H.S. Chai, L.J. Zhao, J.C. He, *Acta Metall. Sin.* **47**, 219 (2011)